

# SOLITON DYNAMICS IN THE MULTIPHOTON PLASMA REGIME

Chad A. Husko<sup>1,\*</sup>, Sylvain Combrié<sup>2</sup>, Pierre Colman<sup>2</sup>,  
Jiangjun Zheng<sup>1</sup>, Alfredo De Rossi<sup>2</sup>, Chee Wei Wong<sup>1,\*</sup>

<sup>1</sup>Optical Nanostructures Laboratory, Columbia University New York, NY 10027 USA

<sup>2</sup>Thales Research and Technology, Route Départementale 128, 91767 Palaiseau, France

*\*Correspondence and requests for materials should be addressed to  
chad.husko@sydney.edu.au (C.A.H.) and cww2104@columbia.edu (C.W.W.)*

## SUPPLEMENTARY INFORMATION

### Linear properties of the photonic crystal waveguide

The transmission of the 1.5-mm photonic crystal (PhC) waveguide is illustrated in Fig. S1(a). Total insertion loss (before and after coupling optics) is estimated to be 13 dB at 1530 nm (group index  $n_g = 5$ ), including 10 dB attributable to the coupling optics, and 1 dB propagation loss at this wavelength. Carefully designed integrated mode-adapters reduce waveguide coupling losses to 2 dB (insertion) and suppress Fabry-Perot oscillations from facet reflections as shown in the inset of Fig. S1(a) [1]. The linear loss is  $\alpha = 10$  dB/cm at 1540 nm, scaled linearly with  $n_g$  [2, 3]. The small feature at 1530 nm is the onset of the higher-order waveguide mode coupling. The energy coupled into the PhC is estimated by assuming symmetric coupling loss (input and output) except for a factor accounting of mode mismatch on the input side (lens to waveguide) that we do not have at the output since  $P_{out}$  is measured with a free space power meter. This enables us to calculate the factor between the measured average power at input (output) and the value of the average power at the beginning (end) of the waveguide. Pulse energy is obtained by dividing by the repetition ratio. As noted in the main body, a slight dip is present in the group index at  $\sim 1545$  nm, implying a small deviation in the local dispersion  $\beta_2$ . This gives rise the the spreading near  $N=2.5$  in Fig. 5(b) corresponding to that wavelength region.

### Frequency-resolved optical gating (FROG) pulse

Fig. S1(b) shows the frequency-resolved optical gating (FROG) setup used in the experiments. With the FROG technique, one is able to completely characterize the pulse, including intensity and phase information in both the spectral and temporal domains. We employed a second-harmonic FROG (SHG FROG) technique detailed in the Methods. The equation governing the second-harmonic generation SHG-FROG is:

$$I_{FROG}(\omega, \tau) = \left| \int_{-\infty}^{\infty} E(t)E(t - \tau)e^{-i\omega t} dt \right|^2, \quad (1)$$

where  $I_{FROG}(\omega, \tau)$  is the measured pulse,  $E(t)$  is the electric field and  $e^{-i\omega t}$  the phase. The spectrograms are processed numerically to retrieve the pulse information [4]. Fig. S2(a) compares the experimental and retrieved spectrograms of typical input pulse measured by the FROG, here at 1533.5 nm. Figs. S2(b) and (c) indicate the FROG autocorrelation and spectrum compared with independent measurements with a commercial autocorrelator (Femtochrome) and optical spectrum analyzer (OSA), respectively. Fig. S2(d) shows the temporal intensity and phase retrieved from the FROG measurement, information unavailable from typical autocorrelation and OSA measurements. The pulse phase is flat across the pulse, indicating near-transform limited input pulses.

### Frequency-resolved optical gating of chip-scale ultrafast solitons at 1533.5 nm and 1546 nm

Fig. S3 shows the retrieved FROG intensity (blue line) and phase (magenta) at 1533.5 nm ( $n_g = 5.4$ ,  $\beta_2 = -0.49$  ps<sup>2</sup>/mm). The nonlinear Schrödinger equation results are presented in Figs. S3 (a)-(d) with predicted intensity (dashed red) and phase (dash-dot black). Since FROG only gives the relative time, we temporally offset the FROG traces to overlap the NLSE for direct comparison. All parameters precisely determined from experimental measurements, e.g. no free fitting parameters. Fig. S3(d) shows the maximum pulse compression to a minimum duration of 440 fs from 2.3 ps ( $\chi_c = 5.3$ ) at 7.7 W (20.1 pJ,  $N = 3.5$ ), demonstrating higher-order soliton compression. The slight dip in the pulse phase at positive delay (temporal tail) is due to free-carrier blue-shift.

Figs. S4(a)-(d) show the FROG traces at 1546 nm as in the main paper. Figs. S4(e)-(h) compare the retrieved FROG spectral density (dotted black) and NLSE simulations (solid

blue) to independent measurements with an optical spectrum analyzer (dashed red). The experimental and modeling results agree simultaneously in both the time (main text) and spectral domains shown here.

**Periodic soliton recurrence and suppression in the presence of free-electron plasma: role of free-carriers and input pulse shape**

In Fig. 4 of the main text, we demonstrated the suppression of periodic soliton recurrence in the presence of free-electron plasma. Fig. S5 shows additional details of the physics presented there. Fig. S5(a) shows the NLSE model of the experimental situation:  $L = 1.5$  mm and free carriers ( $N_c$ ) as in the main paper. Fig. S5(b) shows that even with longer  $L = 3$  mm samples the pulse recurrence is clearly suppressed. Fig. S5(c) shows NLSE modeling in the absence of free-carriers ( $N_c = 0$ ). The pulse splits temporally, but does not reform due to loss. In contrast to the FROG input pulses used in the simulations throughout the text thus far, Figs. S5(d)-(f) show NLSE models with chirp-free *sech*<sup>2</sup> input pulses. Importantly, the same basic features are represented for both the FROG (a)-(c) and *sech*<sup>2</sup> inputs (d)-(f), demonstrating soliton re-shaping of our experimental pulses.

**Pulse acceleration in a multiphoton plasma**

The mechanism accelerating the pulse is a non-adiabatic generation of a free-carrier plasma via multiphoton absorption within the pulse inducing a blue frequency chirp. Fig. S6(a) shows a schematic of the self-induced free-carrier blue-shift and resulting acceleration of the pulse. The regions of largest plasma generation occur at the waveguide input as well as at points of maximum compression as shown in Fig. 3 of the main text. Moreover, we note that the dispersion bands themselves do not shift at our 10-pJ 1550-nm pulse energies, in contrast to other reports with Ti:sapphire pump-probe and carrier injection with above-band-gap 1 to 100 nJ pulse energies at  $\sim 800$ -nm [5, 6]. Such a scenario, presented in Fig. S6(b), would only cause the light to shift slower group velocities, as has been shown in Ref. [5]. Furthermore, this mechanism is not a deceleration, but rather a frequency conversion method to change the pulse central wavelength to a frequency with different propagation properties.

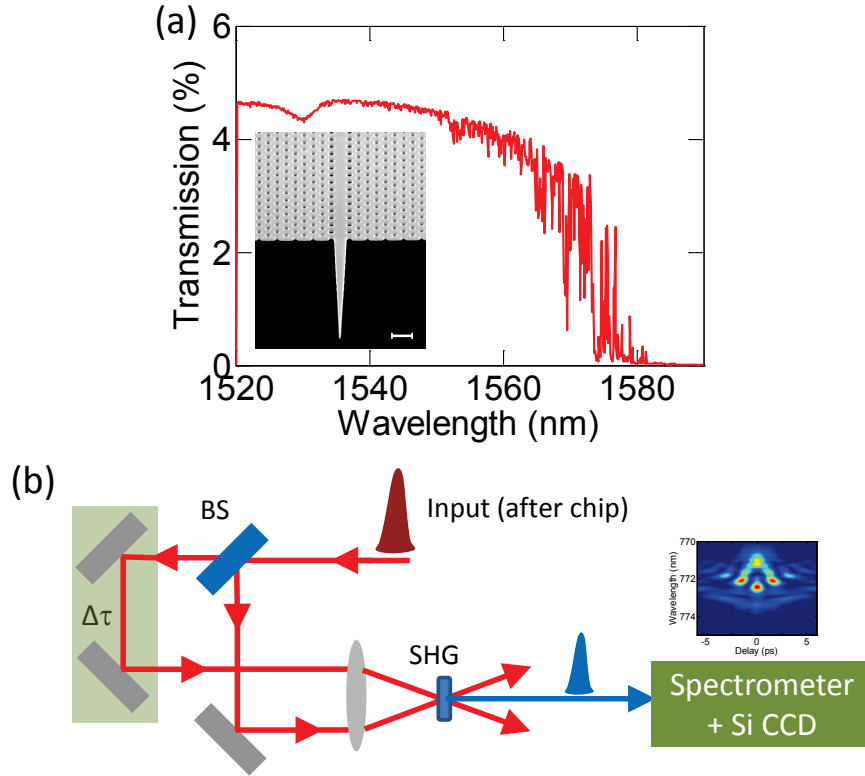


FIG. S1. Linear properties and home-built FROG setup. (a) Linear transmission of the photonic crystal waveguide device. The dip around 1530 nm is the onset of a higher-order mode, outside the regime of interest. (b) Frequency-resolved optical gating (FROG) setup used to characterize the soliton pulse dynamics, including complete intensity, duration, and phase information. BS: Beam splitter, SHG: BBO second-harmonic crystal,  $\Delta\tau$ : delay stage.

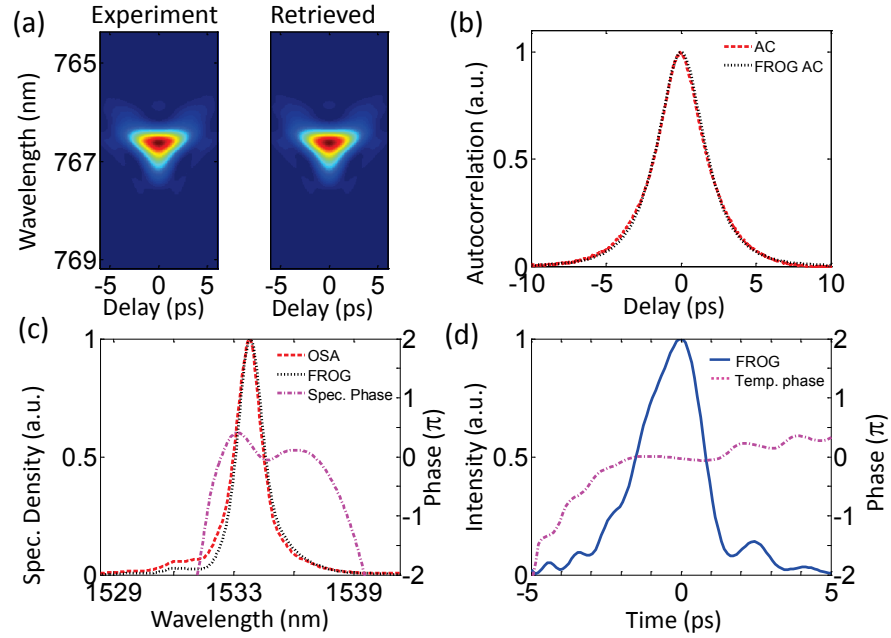


FIG. S2. Typical input pulse measured by the FROG. Though 1533.5 nm is shown here, other wavelengths exhibit similar characteristics. (a) Experimental and retrieved FROG traces (b) Autocorrelation - FROG (black dotted) and autocorrelator (red dashed) (c) Spectral density FROG (black dotted), optical spectrum analyzer (red dashed) and spectral phase (dash-dot magenta) (d) Temporal intensity (solid blue) and phase (dash-dot magenta).

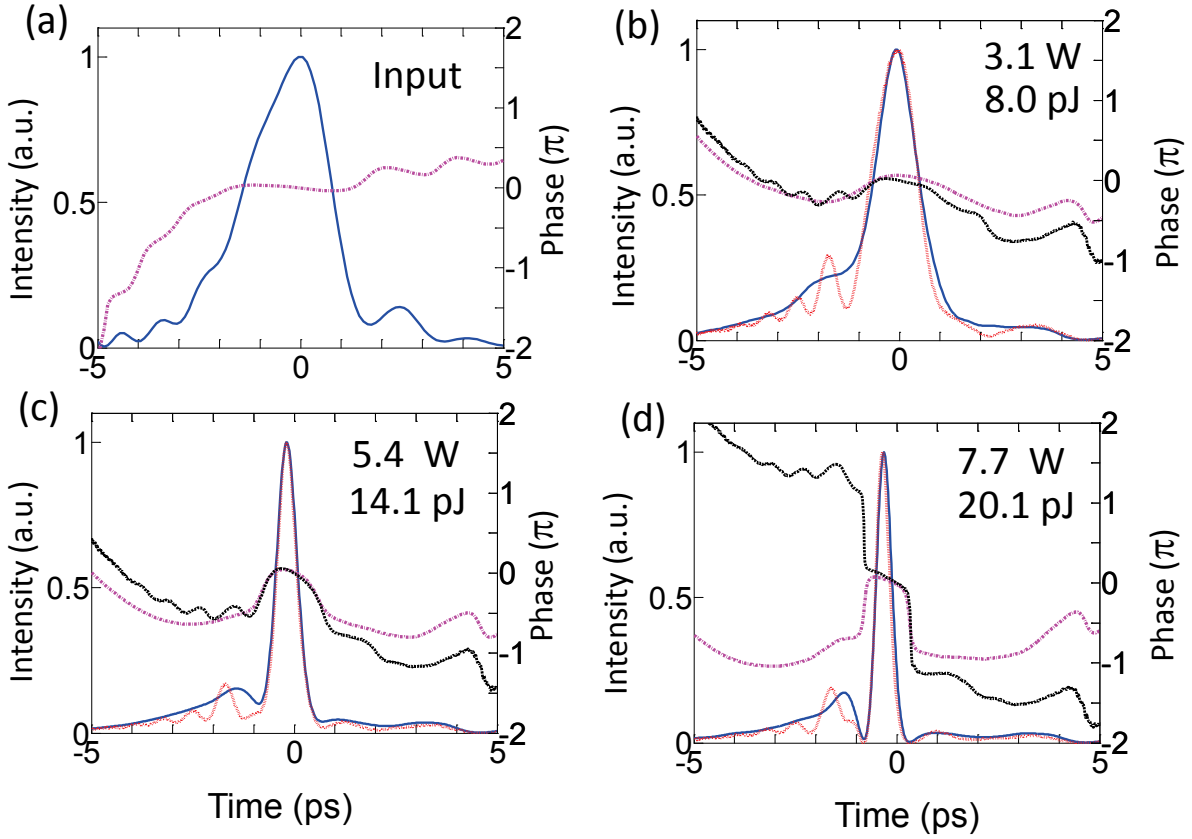


FIG. S3. Ultrafast soliton compression at 1533.5 nm. Panels (a)-(d) correspond to the spectrograms in Figs. 2(i)-(l) in the main text. (a)-(d): FROG retrieved time domain intensity (solid blue) and phase (dashed magenta), with gating error less than 0.005 on all runs. Superimposed nonlinear Schrödinger equation modeling: intensity (dashed red), and phase (dash-dot black), demonstrates strong agreement with experiments. Panel (d): The pulse compresses from 2.3 ps to a minimum duration of 440 fs ( $\chi_c = 5.3$ ) at 20.1 pJ (7.7 W), demonstrating higher-order soliton compression.

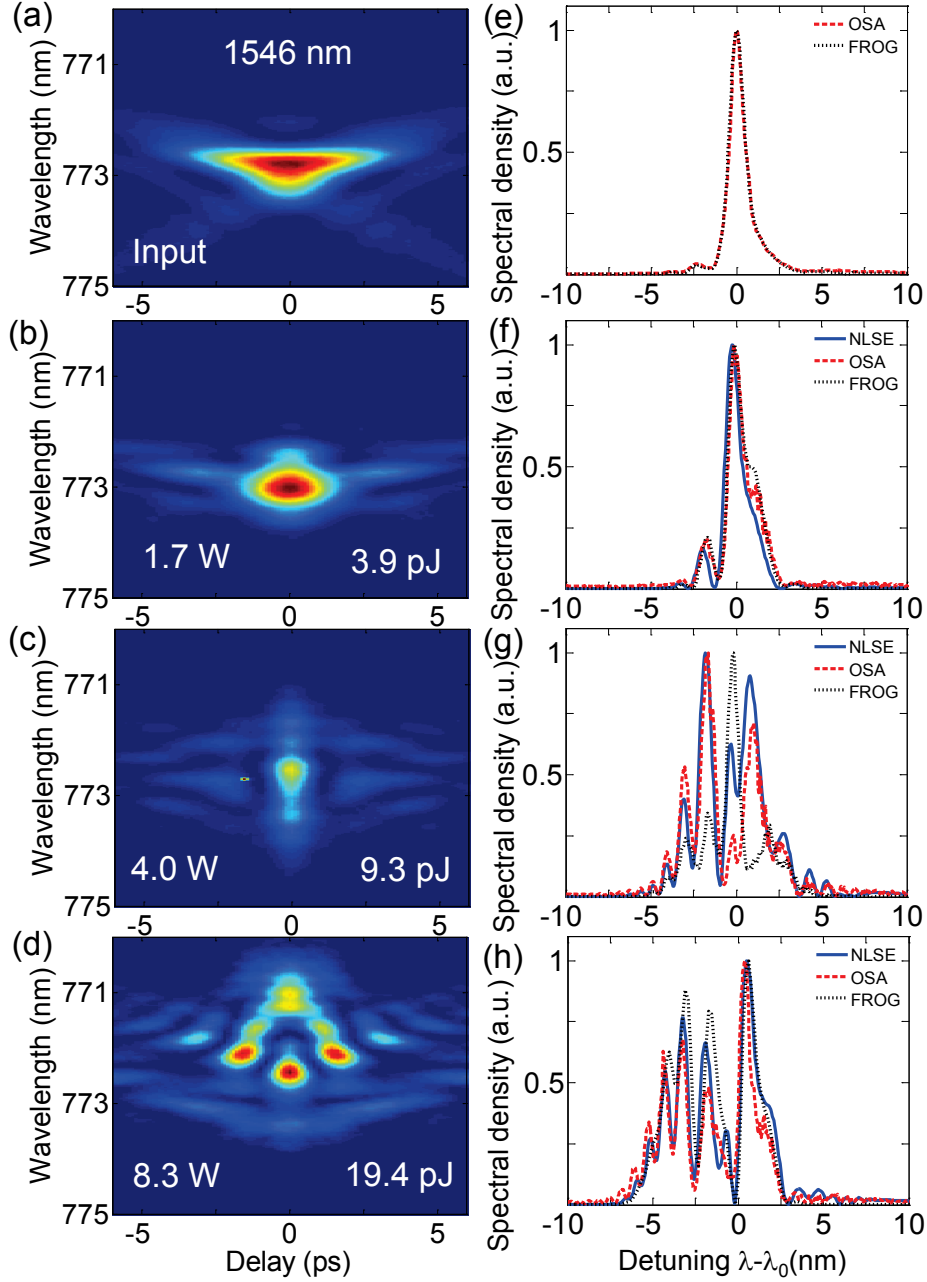


FIG. S4. Spectral properties of pulses at 1546 nm. (a)-(d): FROG spectrograms with coupled pulse energies from 3.9 pJ to 20.1 pJ repeated from the main text for simple comparison. (e)-(h): FROG retrieved spectral density (dashed black), OSA (dashed red), and superimposed NLSE modeling (solid blue) demonstrate agreement in both the spectral domain (shown here) and time domain (main text).

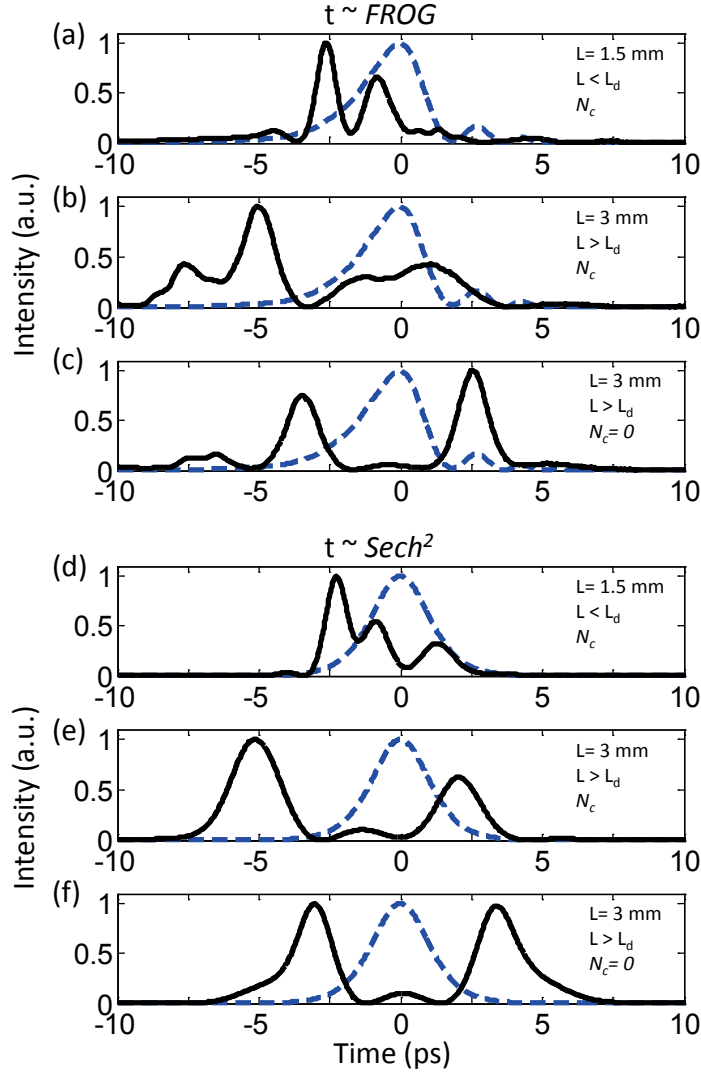


FIG. S5. Suppression of soliton periodic recurrence: role of free-carriers and input pulse shape. Panels (a)-(c): NLSE with experimental FROG input pulse. (a) Full simulation  $L = 1.5$  mm and free carriers ( $N_c$ ) as in the main paper. (b)  $L = 3$  mm with free-carriers ( $N_c$ ). (c)  $L = 3$  mm with suppressed free-carriers ( $N_c = 0$ ). Panels (d)-(f), same as (a)-(c) with NLSE with  $sech^2$  input pulse.



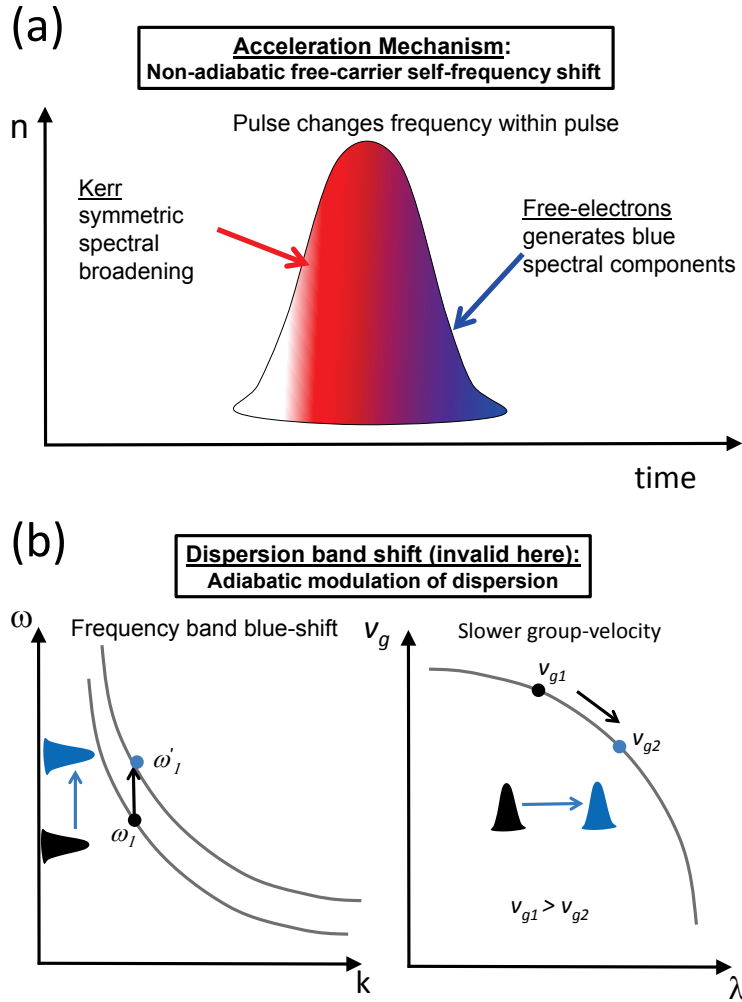


FIG. S6. Pulse modulation mechanisms. (a) Acceleration is due to the self-induced frequency-chirp due to non-adiabatic free-carrier generation within the pulse. This is confirmed via the NLSE simulations in the paper. (b) Dispersion band-shift due to adiabatic modulation of free-carriers at large intensities induces a frequency conversion process. This is not the case here.

- 
- [1] Q. V. Tran, S. Combrié, P. Colman, and A. De Rossi, “Photonic crystal membrane waveguides with low insertion losses,” *App. Phys. Lett.* **95**, 061105 (2009).
- [2] T. Baba, “Slow light in photonic crystals,” *Nature Photonics* **2**, 465 (2008).
- [3] C. Monat, B. Corcoran, M. Ebnali-Heidari, C. Grillet, B. Eggleton, T. White, L. O’Faolain, and T. F. Krauss, “Slow light enhancement of nonlinear effects in silicon engineered photonic crystal waveguides,” *Opt. Express* **17**, 2944 (2009).
- [4] R. Trebino, *Frequency-resolved optical gating: the measurement of ultrashort laser pulses* (Kluwer, 2002).
- [5] T. Kampfrath, D. M. Beggs, T. P. White, A. Melloni, T. F. Krauss, and L. Kuipers, “Ultrafast adiabatic manipulation of slow light in a photonic crystal,” *Phys. Rev. A* **81**(4), 043837 (2010).
- [6] S. W. Leonard, H. M. Van Driel, J. Schilling, and R. B. Wehrspohn, “Ultrafast band-edge tuning of a two-dimensional silicon photonic crystal via free-carrier injection,” *Phys. Rev. B* **66**, 161102 (2002).